NUMERICAL SIMULATION OF KATABATIC WIND AT MIZUHO STATION, EAST ANTARCTICA

Takashi ADACHI

Research Institute of Japan Weather Association, Kaiji Center Bldg., 5, Koji-machi 4-chome, Chiyoda-ku, Tokyo 102

and

Sadao KAWAGUCHI

National Institute of Polar Research, 9–10, Kaga 1-chome, Itabashi-ku, Tokyo 173

Abstract: Twenty-six pairs of vertical profiles of wind vectors and air temperatures for typical katabatic winds are chosen from about 70 aerological data of low altitude radiosondes and automatic tracking systems at Mizuho Station, East Antarctica during 1980 (as observed by S. KAWAGUCHI *et al.*: Mem. Natl Inst. Polar Res., Spec. Issue, **24**, 77, 1982), and averaged after normalization using katabatic wind layer thickness, surface wind vector, and difference of potential temperature between the top of the katabatic wind layer and the surface.

The wind spiral, vertical profiles of the two horizontal wind components, eddy diffusivity, friction velocity, heat flux and local Monin-Obukhov length are calculated with the numerical model of stationary katabatic winds developed by T. ADACHI (Antarct. Rec., **67**, 64, 1979) where not only the two wind components but also eddy diffusivity are unknown. Therefore, this model is superior to the simple K-theory with a known eddy diffusivity.

Numerical solutions for katabatic wind profiles agree well with the above-mentioned averaged profiles observed at Mizuho Station.

1. Introduction

Aerological observations (KAWAGUCHI *et al.*, 1982) were carried out 79 times at Mizuho Station (70°41′53″S, 44°19′54″E, 2230 m a.s.l.) in the Cold Katabatic zone, during the wintering of the 21st Japanese Antarctic Research Expedition (January 1980–January 1981).

Mizuho Station (Fig. 1) is on the antarctic ice sheet which is a horizontally uniform ice slope, where katabatic winds blow down day and night year round and the constancy of the surface winds and directions is very high, especially in winter (SASAKI, 1974).

According to SHIMIZU *et al.* (1978), the ice slope in Mizuho Plateau varies from 2.2×10^{-3} to 5×10^{-2} radian. INOUE *et al.* (1983) used 3.9×10^{-3} radian. However, there is no accurate measurement of the average ice slope angle in the up-wind direction at Mizuho Station yet.

The vertical structure of katabatic winds on the Mizuho Plateau was studied by KOBAYASHI (1978). Recently ADACHI (1984a, b) has presented new analytical solutions

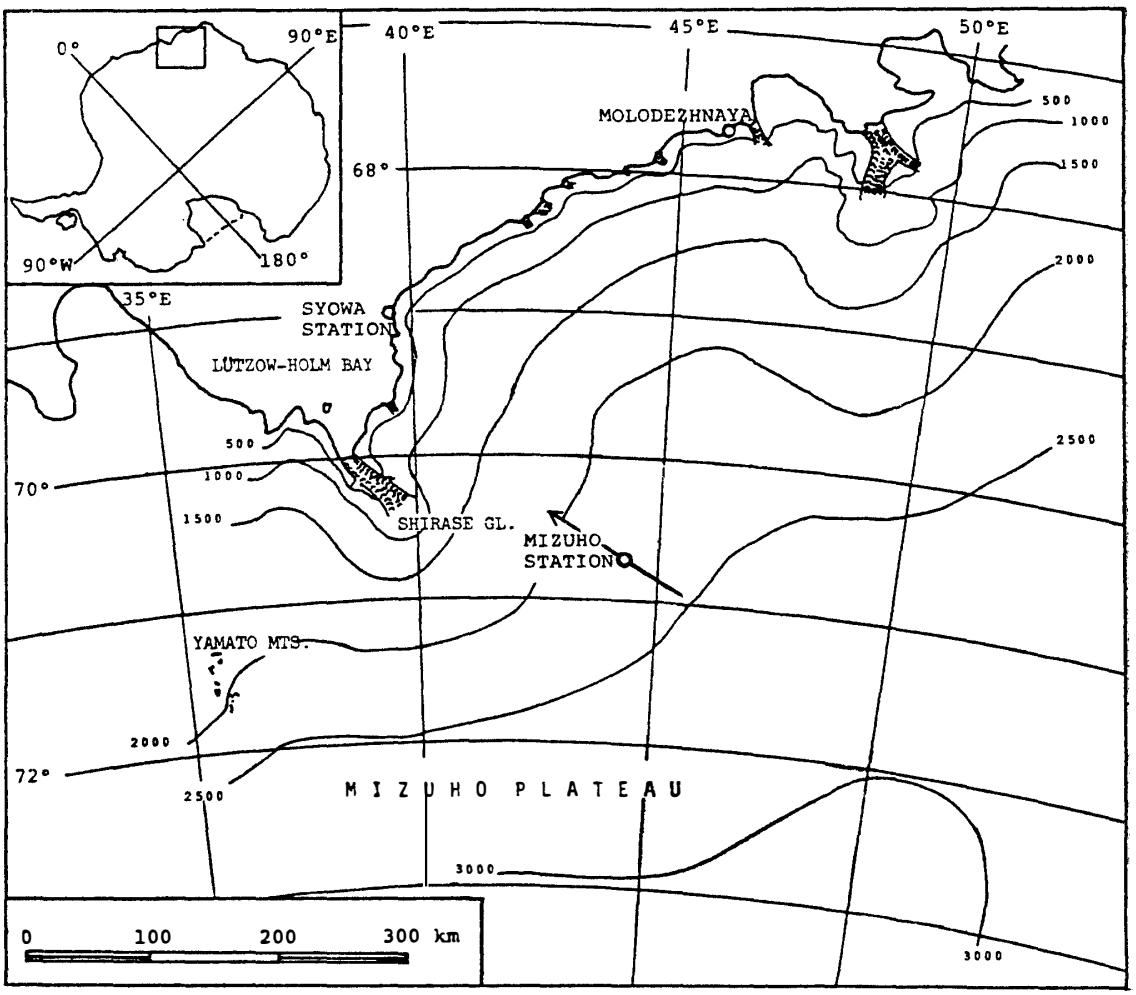

Fig, 1. Location of Mizuho Station. The arrow indicates the direction of the slope near this station which is about 300 degrees from true North. The slope is around 3×10^{-3} *radian. This map is partially modified from the one of* SATOW *et al. (1983).*

of katabatic winds at Mizuho and Syowa Stations with constant eddy diffusivity and realistical vertical profile of pressure gradient.

ADACHI (1979) presented a numerical model of katabatic wind in which not only the two wind components but also eddy diffusivity is a dependent variable. ADACHI (1983) did a numerical simulation of the strong katabatic wind profile observed on 1420 LT, April 23, 1973 at Mizuho Station (KOBAYASHI and YOKOYAMA, 1976).

In this investigation, we present a pair of averaged vertical profiles of horizontal wind components and potential temperature in a typical katabatic wind at Mizuho Station in 1980, numerically simulate these averaged katabatic wind component profiles, and predict the eddy diffusivity, friction velocity and heat flux which were not observed in this case.

2. Observed Data and Preliminary Analysis

Aerological data of low altitude radiosondes and automatic tracking systems at Mizuho Station in 1980 (KAWAGUCHI *et al.*, 1982) and surface layer data of meteorological towers at Mizuho Station in 1980 (OHATA *et al.*, 1981, 1983) are used in this study to analyze typical katabatic winds. The following aerological data were selected for this study:

(a) Height of maximum wind speed is not more than 130 m from snow surface.

(b) Vertical profile of wind speed has a sharp peak.

(c) Vertical profile of potential temperature has a large positive gradient in the surface layer.

An example of the wind aloft and potential temperature profiles in a typical katabatic wind at Mizuho Station is shown in Fig. 2a. Note that the maximum wind speed is about 70 m from the snow surface and the vertical wind speed profile has a sharp peak at this height. The wind direction below 500 m is nearly ESE. The

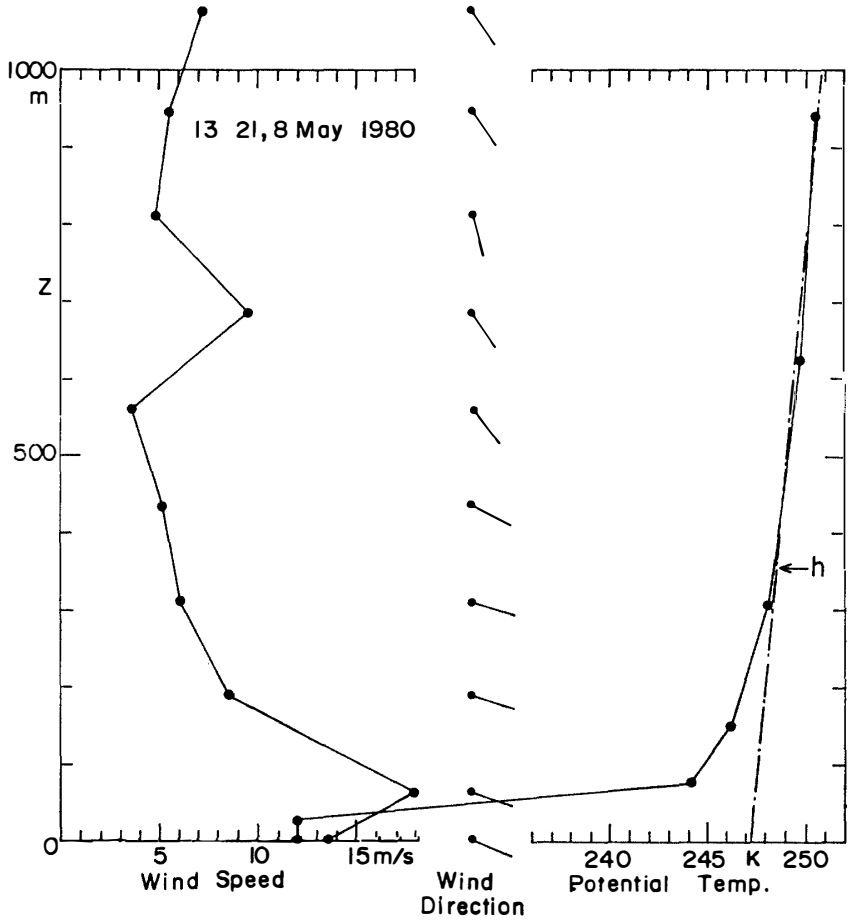

Fig. 2a. Example of wind aloft and potential temperature profile for a typical katabatic wind with a maximum wind speed height up to 130 m at Mizuho Station. h: Thickness of katabatic wind layer, —·—: estimated undisturbed potential temperature.

vertical potential temperature profile has a large positive gradient below 200 m, which indicates strong stability in this layer. 26 sets of data similar to Fig. 2a were obtained at Mizuho Station in 1980.

Potential temperatures undisturbed by the ice slope (Θ) are estimated by fitting to the observed potential temperatures in the layer above the katabatic wind layer and extrapolating linearly to the surface as shown by the chained line in Fig. 2a.

The top of the katabatic wind layer (h) is defined by the intersection of this profile of undisturbed potential temperature and that of the observed profile shown by the arrow in Fig. 2a. h is also called the thickness of the katabatic wind layer.

Another example of katabatic wind at Mizuho Station is shown in Fig. 2b. As in Fig. 2b, the height of the maximum wind speed is about 250 m, and the vertical wind speed profile has no sharp peak at this height because large scale motion affects the flow in the atmospheric boundary layer. However, we can estimate the undisturbed potential temperatures and katabatic wind layer thickness by the same procedure as in Fig. 2a. 7 sets of data similar to Fig. 2b were obtained at Mizuho Station in 1980.

A comparison with the top of the katabatic wind layer (h) and the top of the surface inversion layer of air temperature (h_i) is shown in Fig. 3. When one or more inversion layers are superposed above the surface inversion layer, h may not

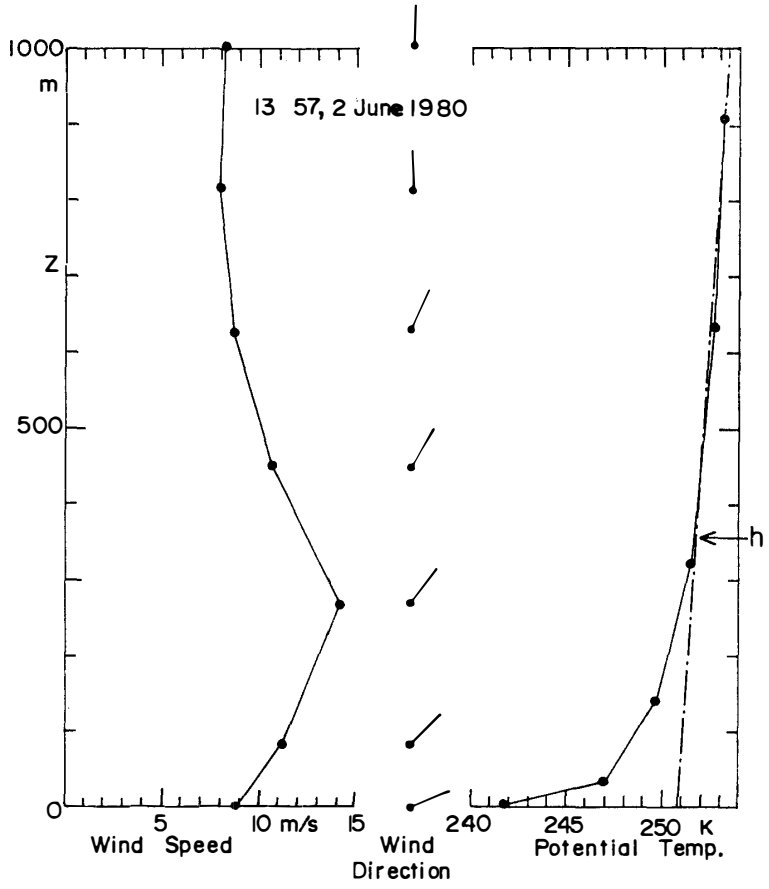

Fig. 2b. Same as Fig. 2a but for a katabatic wind with a maximum between 130 and 500 m.

agree with the h_i. However, as in Fig. 3, the h and h_i almost coincided except in three cases for which there were not enough observed points.

In this research h is adopted for the following analyses.

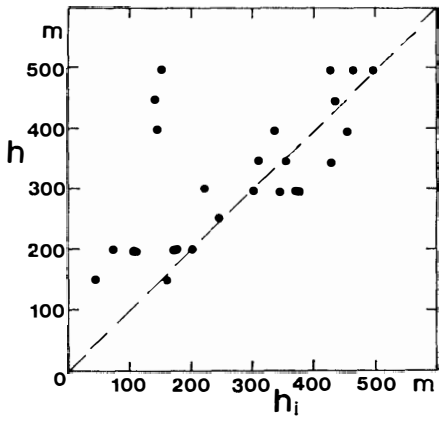

Fig. 3. Top of katabatic wind layer (h) vs. the top of surface inversion layer of air temperature (h_i).

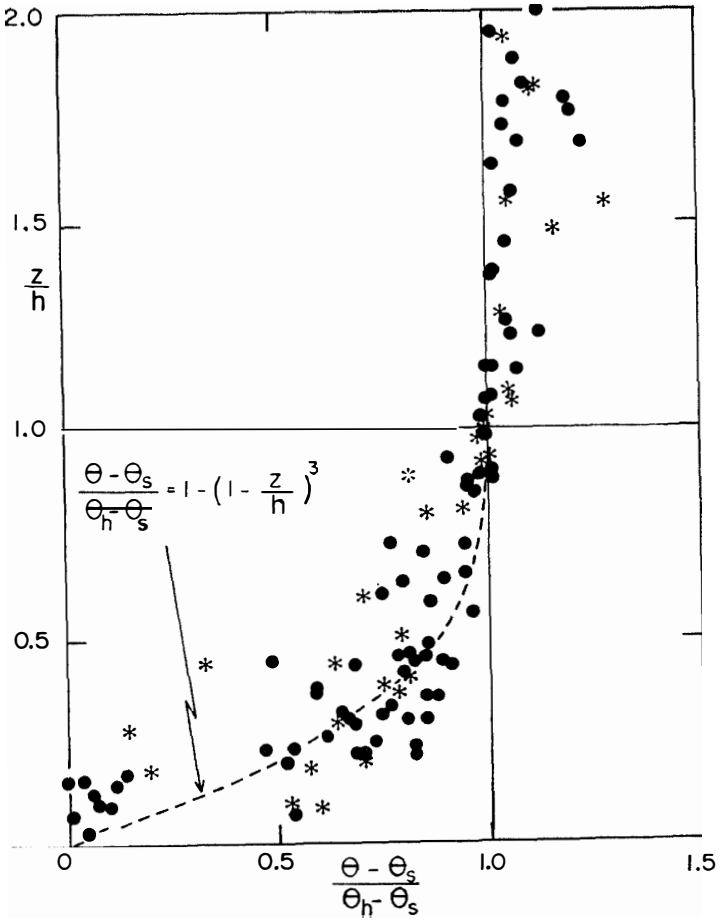

Fig. 4. Normalized potential temperature profile. z: Height above snow surface, h: thickness of katabatic wind layer, θ: potential temperature, θ_s: $\theta=\theta_s$, $z=1.7$ m, θ_h: $\theta=\theta_h$, $z=h$, ●: observed data in the similar cases to Fig. 2a (26 cases), ∗: observed data in the similar cases to Fig. 2b (7 cases).

3. Averaged Profile of Potential Temperature

As one of the purposes of this study is to present the average profile of potential temperature in a typical katabatic wind, the data at first were plotted in the non-dimensional coordinates z/h and $(\theta-\theta_s)/(\theta_h-\theta_s)$. The symbols are explained in the explanation of Fig. 4. The dashed line in Fig. 4 indicates an equivalent equation to the one proposed by YAMADA (1979) in the case of the nocturnal surface inversion over flat terrain. As is evident from Fig. 4 this empirical formula for vertical potential temperature profile is also good over sloping ice.

We read by the eye block means of observed values indicated by black circles in Fig. 4. Data indicated by asterisks are neglected in this reading because we seek average values in a typical katabatic wind.

Thereafter, we obtained the averaged potential temperature profile by calculation using averaged values of h, θ_h and θ_s which are 325 m, 252.2 K and 236.4 K, respectively. The vertical profile of potential temperature $(\theta-273)$ is shown in Fig. 5a. The chained straight line in Fig. 5a indicates the undisturbed potential temperature profile $(\Theta-273)$ estimated in the same way as Fig. 2a.

Figure 5b shows the effect of the cold sloping surface (v_k) which has dimensions of wind speed and is calculated by the following equations using the values of θ and Θ in Fig. 5a:

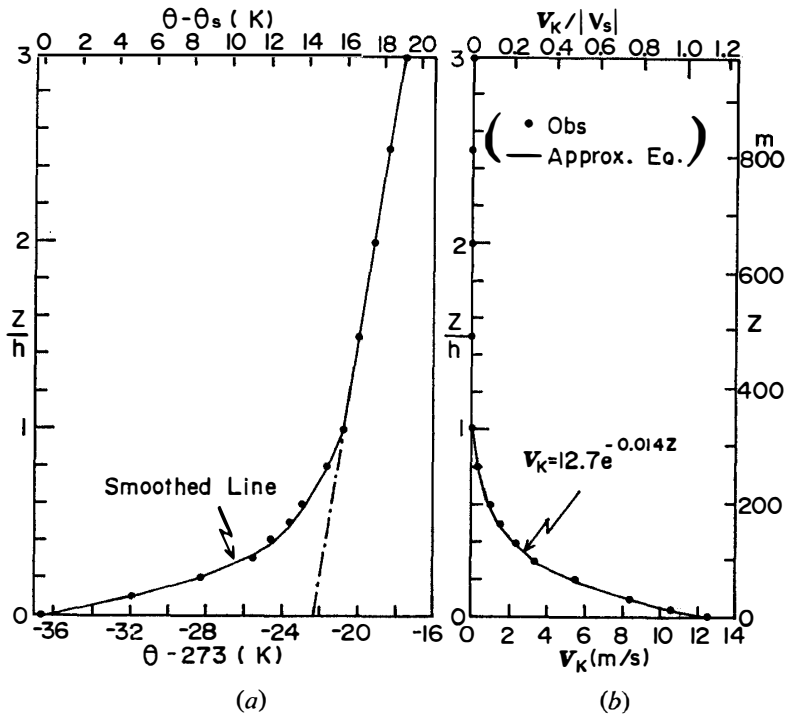

Fig. 5. *(a) Averaged potential temperature profile. The black circles indicate the averaged value. The solid line indicates smoothed values. The chained straight line indicates undisturbed potential temperature; Θ.*
(b) Vertical profile of effect of cold sloping surface (v_k). $v_k=(g/f)(\Delta\theta/\bar{\Theta})\sin\gamma_0$, $\Delta\theta=\theta-\Theta$, V_s: averaged surface wind vector.

$$v_k=(g/f)(\Delta\theta/\bar{\Theta})\sin\gamma_0, \quad (1)$$

$$\Delta\theta=\theta-\Theta, \quad (2)$$

$$g=9.8\,\mathrm{m/s^2}, \quad (3)$$

$$f=-1.4\times10^{-4}\,\mathrm{s^{-1}}, \quad (4)$$

$$\bar{\Theta}=(\theta_h+\theta_s)/2=244.3\,\mathrm{K}, \quad (5)$$

$$\gamma_0=3\times10^{-3}\,\mathrm{rad}, \quad (6)$$

g: Gravity acceleration,
f: Coriolis parameter,
$\bar{\Theta}$: Mean potential temperature.

Equation (1) indicates that v_k is the thermal wind due to the cold sloping surface but does not include geostrophic wind shear due to large-scale motion.

The solid line in Fig. 5b indicates the following empirical formula:

$$v_k=12.7\exp(-0.014z). \quad (7)$$

The units of v_k and z are m/s and m, respectively. If v_k is the cross slope components, it is clear that the down slope component (u_k) is zero.

4. Analysis of Wind Data

As in Fig. 6, two coordinate systems are used in this paper. (u_1, v_1) is called the A-coordinate system and is mainly used to analyze wind data. (u, v) is called the B-coordinate system and is used for numerical simulations of wind profiles.

The A-coordinate system, surface wind vectors and katabatic wind layer thickness are used to normalize vertical profiles of horizontal wind components. Data of 26 cases similar to Fig. 2a are plotted in Figs. 7a and 7b. Micrometeorological tower wind data are also plotted. The solid lines in these figures are smoothed lines which are taken to be averaged values.

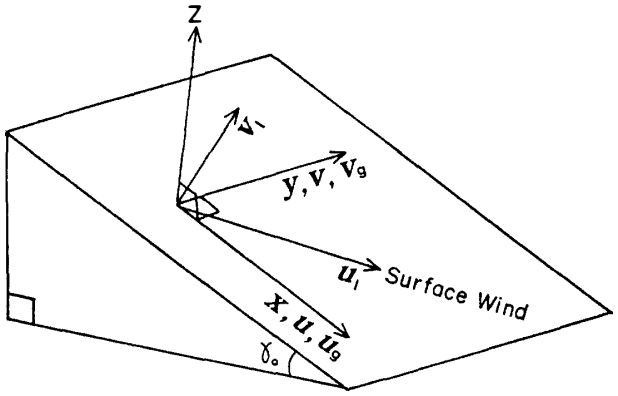

Fig. 6. Coordinate systems. (u_1, v_1): A-coordinate system, (u, v): B-coordinate system, u_1: wind component of the surface wind direction, v_1: $v_1\perp u_1$, u: down slope wind component, v: cross slope wind component ($v\perp u$), z: normal to slope, γ_0: surface slope.

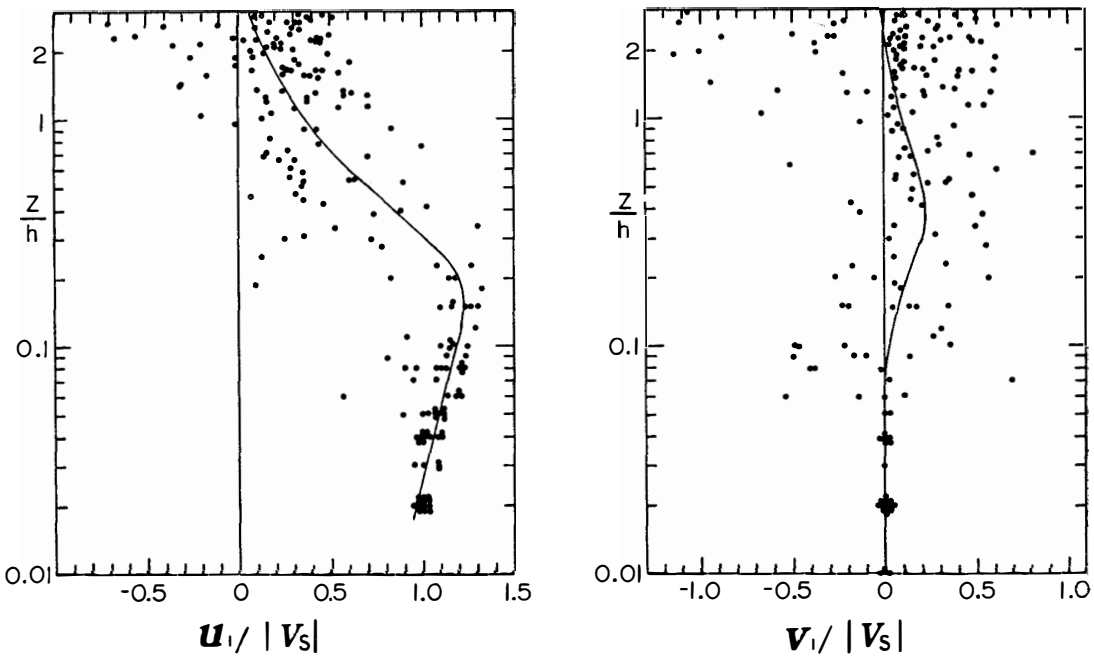

Fig. 7. (*a*) *Normalized u-component profile.* $|V_s|$*: Magnitude of surface wind vector,* ●*: observed data in the similar cases to Fig. 2a,* —*: smoothed line.*
(*b*) *Same as Fig. 7a, but for* v_1.

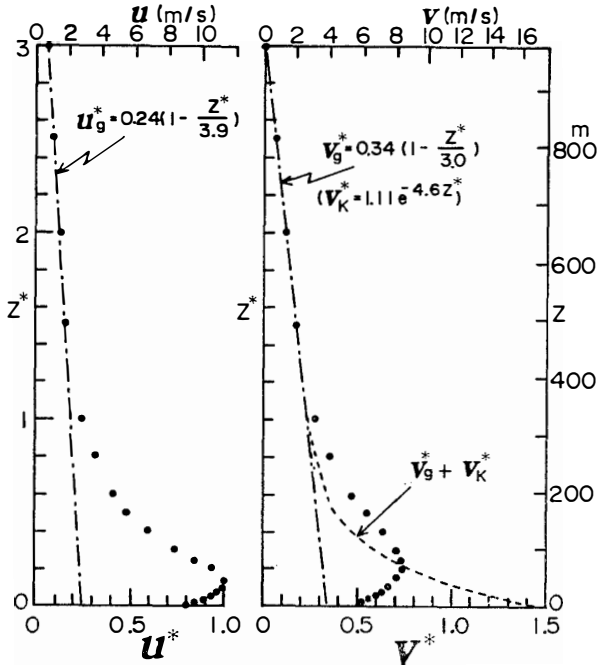

Fig. 8. Averaged u- and v-components profiles of wind and geostrophic wind in B-coordinate system.
$u_g^*=u_g/|V_s|$, $v_g^*=v_g/|V_s|$, $z^*=z/h$, $u^*=u/|V_s|$, $v^*=v/|V_s|$, $v_k^*=v_k/|V_s|$, ●*: observed wind components,* —·—*: estimated geostrophic wind components,* ----*: resultant of* v_g^* *and* v_k^*.

Averaged wind components in the A-coordinate system can be transformed into the B-coordinate system by a simple calculation. The results of this coordinate transformation are shown in Fig. 8.

Geostrophic wind components (u_g and v_g) of the B-coordinate system are estimated by fitting to the above-mentioned wind components in a range of non-dimensional heights (z/h) from 1.5 to 3.0 which is clearly above the slope wind layer and extrapolating linearly to the surface. As in Fig. 8 the geostrophic wind components are estimated as follows:

$$u_g^* = 0.24\ (1 - z^*/3.9), \tag{8}$$

$$v_g^* = 0.34\ (1 - z^*/3.0). \tag{9}$$

In order to obtain dimensional values the following relations are used:

$$u_g = u_g^* |\bar{V}_s|, \tag{10}$$

$$v_g = v_g^* |\bar{V}_s|, \tag{11}$$

$$|\bar{V}_s| = 11.4\ \mathrm{m/s}, \tag{12}$$

$$z = z^* \bar{h}, \tag{13}$$

$$\bar{h} = 325\ \mathrm{m}, \tag{14}$$

$$u = u^* |\bar{V}_s|, \tag{15}$$

$$v = v^* |\bar{V}_s|, \tag{16}$$

$$v_k = v_k^* |\bar{V}_s|. \tag{17}$$

Equation (7) is also converted into the following non-dimensional equation:

$$v_k^* = 1.11 \exp(-4.6 z^*). \tag{18}$$

The sum of v_g^* and v_k^* is illustrated by the dashed line in Fig. 8. This sum represents the y-component of the geostrophic wind balanced with the effective pressure gradient in the katabatic wind layer. In other word, $v_g^* + v_k^*$ is the sum of the large scale pressure gradient in the x-direction and the buoyancy force of the cold air mass over the inclined surface. u_g and $v_g + v_k$ are used as input data of numerical simulations of katabatic winds which will be mentioned later.

5. Numerical Simulation of Katabatic Wind

5.1. Governing equations

The numerical simulation model was developed and applied by ADACHI (1979, 1982, 1983). Characteristics of this model are that the effects of atmospheric stability, baroclinicity and the cold sloping surface are considered and not only two wind components but also eddy diffusivity are treated as unknowns in the non-linear differential equations. Therefore this model is different from one with constant K.

The present assumptions are:

(a) The flow is stationary.

(b) The z-component of the wind vector is zero on the sloping terrain.

(c) The wind vector is independent of x and y.

(d) Monin-Obukhov's similarity theory holds at each height of the atmospheric boundary layer.

(e) The local Monin-Obukhov length is defined by the heat and momentum flux in each height layer.

The coordinate system used in this model is the B-coordinate system in Fig. 6. The z-coordinate is approximately vertical as the surface slope near Mizuho Station is very small. However, the x-component of gravity cannot be neglected as the sloping surface is very long and wide. Moreover, the Coriolis force can not be neglected.

The governing equations are:

$$0=\frac{\mathrm{d}}{\mathrm{d}z}\left(K\frac{\mathrm{d}u}{\mathrm{d}z}\right)+f(v-v_g)+g\cdot\sin\gamma\cdot(\Theta-\theta)/\bar{\Theta}, \tag{19}$$

$$0=\frac{\mathrm{d}}{\mathrm{d}z}\left(K\frac{\mathrm{d}v}{\mathrm{d}z}\right)-f(u-u_g), \tag{20}$$

$$K=kz|\boldsymbol{\tau}/\rho|^{1/2}/\phi, \tag{21}$$

$$\phi=(1+12z/L)^{1/2}, \tag{22}$$

$$\boldsymbol{\tau}/\rho=K\frac{\mathrm{d}\boldsymbol{V}}{\mathrm{d}z}, \tag{23}$$

$$q/C_p\rho=-K\frac{\mathrm{d}\theta}{\mathrm{d}z}, \tag{24}$$

$$z/L=-k(g/\theta)(q/C_p\rho)z/|\boldsymbol{\tau}/\rho|^{3/2}, \tag{25}$$

$$\boldsymbol{V}=u+iv, \tag{26}$$

$$\boldsymbol{V}_g=u_g+iv_g, \tag{27}$$

$$\boldsymbol{\tau}=\tau_x+i\tau_y, \tag{28}$$

$$u_{gk}=u_g, \tag{29}$$

$$v_{gk}=v_g+v_k, \tag{30}$$

$$v_k=-(g/f)\cdot\sin\gamma\cdot(\Theta-\theta)/\bar{\Theta}, \tag{31}$$

$$\boldsymbol{V}_{gk}=u_{gk}+iv_{gk}, \tag{32}$$

$$|\boldsymbol{V}|=\sqrt{u^2+v^2}, \tag{33}$$

$$|\boldsymbol{V}_{gk}|=\sqrt{u_{gk}^2+v_{gk}^2}, \tag{34}$$

$$|\boldsymbol{\tau}|=\sqrt{\tau_x^2+\tau_y^2}, \tag{35}$$

$$i=\sqrt{-1}. \tag{36}$$

Symbols

x: Along slope coordinate (see Fig. 6),
y: Rectangular to x (see Fig. 6),
z: Normal coordinate to x-y plane (see Fig. 6),
u: Wind component (x-axis),
v: Wind component (y-axis),

K: Eddy diffusivity,
f: Coriolis parameter ($f<0$),
g: Gravity acceleration,
Θ: Undisturbed potential temperature,
θ: Potential temperature,
$\overline{\Theta}$: Mean potential temperature,
γ: Slope of flow line,
u_g: Geostrophic wind component (x-axis),
v_g: Geostrophic wind component (y-axis),
k: Von Karman constant ($k=0.41$),
ϕ: Non-dimensional wind shear function,
L: Local value of Monin-Obukhov length,
$\boldsymbol{\tau}$: Shear stress vector,
ρ: Air density,
q: Heat flux,
C_p: Specific heat,
z_0: Roughness length,
$\boldsymbol{V}$: Wind vector,
$\boldsymbol{V}_g$: Geostrophic wind vector,
v_k: Effect of cold sloping surface,
$\boldsymbol{V}_{gk}$: Resultant vector of geostrophic wind vector and effect of cold sloping surface.

Equations (19) and (20) are the equations of the air motions. The third term of eq. (19) or eq. (31) represents the effect of the cold sloping surface, that is, the equivalent geostrophic wind balanced with the component of the buoyancy force along the slope. This component causes the katabatic wind.

Equations (21) and (23) are the relation of eddy diffusivity and shear stress at each level. Equation (22) gives a non-dimensional wind shear function, which was developed and tested for the baroclinic and neutral of stable atmospheric boundary layer by ADACHI (1979, 1983). Moreover, eq. (22) was applied to the strong katabatic winds at Syowa and Mizuho Stations by ADACHI (1983).

5.2. Boundary conditions and input data

5.2.1. Boundary conditions

(a) $\boldsymbol{V}=0$, at $z=z_0$

(b) $\boldsymbol{V}=\boldsymbol{V}_g$, at $z\to\infty$

(c) $\dfrac{d\boldsymbol{V}}{dz}=\dfrac{d\boldsymbol{V}_g}{dz}$ or $\dfrac{\boldsymbol{\tau}}{\rho}=0$, at $z\to\infty$

5.2.2. Input data

(a) Potential temperature profile $\theta(z)$

The observed potential temperature profile is used in this model to avoid increase of the number of parameters in the model.

(b) Geostrophic wind profile $\boldsymbol{V}_g(z)$

As vertical profiles of the horizontal pressure gradient were not observed on the

Mizuho Plateau, the geostrophic winds are estimated by fitting to the observed wind components in the upper layer and extrapolating linearly to the surface.

In the first numerical simulation this upper layer is taken to be from about 500 to 1000 m above the snow surface (eqs. (8) and (9)).

In the second case this upper layer is taken to be near the top of the katabatic wind layer which is 325 m above the snow surface (eqs. (37) and (38)).

(c) Slope of flow lines (γ)

According to KOBAYASHI (1978), the slope of the ice sheet (γ_0) near Mizuho Station is around 3×10^{-3}. The slopes of flow lines in the upper layer are horizontal, while those in the surface layer are equal to the slope of the terrain. Therefore the slopes of flow lines should be a function of height.

However, as the z-component of wind vector is neglected in the present model and the katabatic wind layer thickness is not large, we use the approximation $\gamma=\gamma_0$ in calculating of the meteorological effect of the cold sloping surface.

(d) Effect of clod sloping surface $v_k(z)$

Equations from (1) to (6) in Section 3 are used.

(e) Parameters of non-dimensional wind shear function (ϕ)

Three cases of the parameters of this shear function shown by the solid lines in Fig. 9 were tested in this research. The case of KONDO *et al.* (1978) is also shown by the dashed line for comparison.

(f) Roughness length (z_0)

The aerodynamical roughness length on the snow or ice surface at Mizuho Plateau is very small and variable. Therefore, the following values of the z_0 were tested: $z_0=10^{-2}$ and 10^{-3} cm.

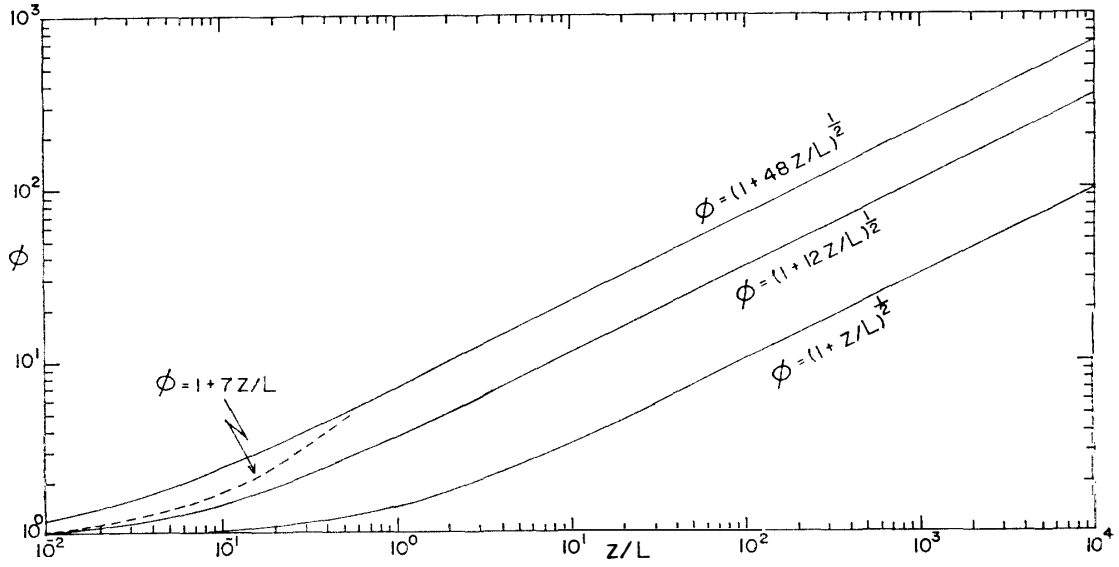

Fig. 9. Non-dimensional wind shear functions (ϕ) vs. atmospheric stability (z/L). $\phi=(1+\alpha z/L)^{\frac{1}{2}}$; $\alpha=1$ or 12 or 48, $\beta=1/2$, the ϕ with $\alpha=12$ and $\beta=1/2$ is presented by ADACHI (1979, 1982), the ϕ with $\alpha=7$ and $\beta=1$ is presented by KONDO et al. (1978).

5.3. Computation procedure

The non-linear differential eqs. (19) to (25) with seven unknown variables; u, v, K, ϕ, τ, q, L were solved by numerical computational method. The only independent variable is z.

The computational method was a combination of successive iteration and the successive relaxation method employed by ADACHI (1979, 1982, 1983).

6. Results and Discussion

6.1. Case-1

The first case of the geostrophic wind components described in the Section 5.2 are represented by eqs. (8) and (9), which are used for the case-1 computation.

The comparison of the three calculated profiles of the down slope wind components with the observed profiles is shown in Fig. 10a. The calculations for the three cases α; $\alpha=1$, 12, 48 are underestimated. The same comparison for the cross slope wind components is illustrated in Fig. 10b. As in Fig. 10b the calculation with $\alpha=12$ best fits the observations.

The probable reason for underestimation of the u-component is that the esti-

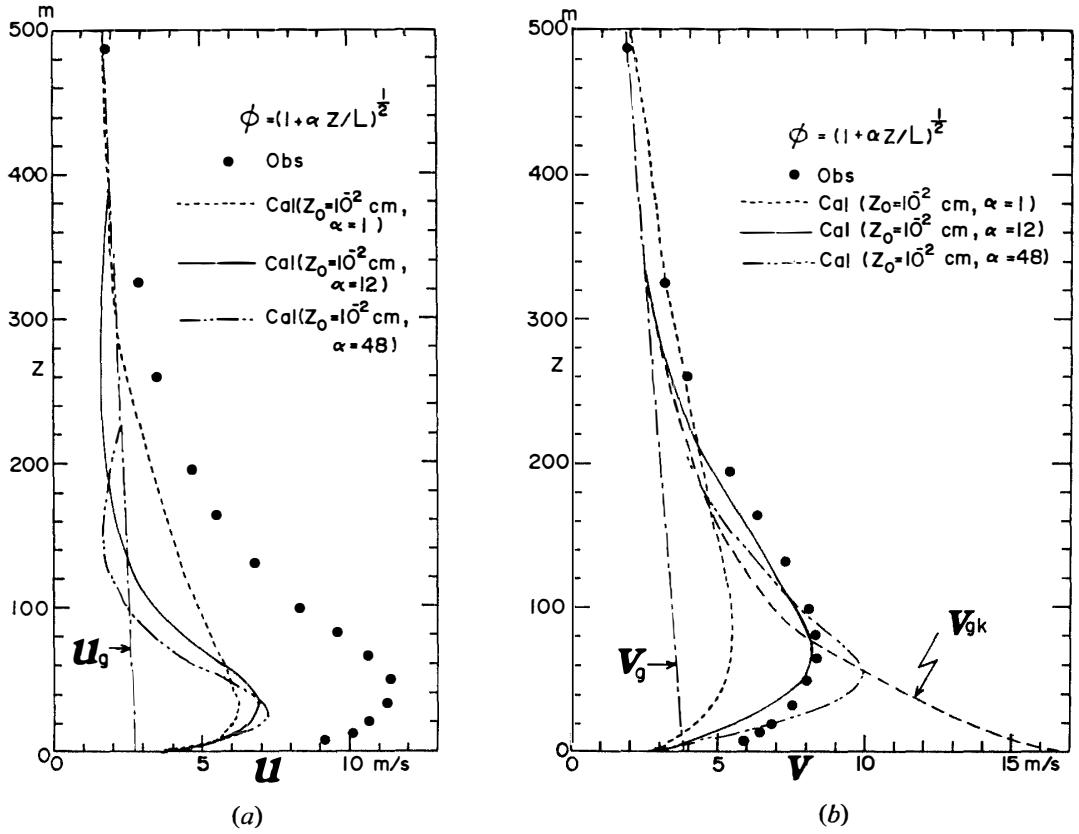

Fig. 10. (*a*) *Calculated down slope wind component profiles vs. observed profile in case-1.* —·—: *Geostrophic wind component* (u_g).
(*b*) *Calculated cross slope wind component profiles vs. observed profile in case-1.* —·—: *Geostrophic wind component* (v_g).

mated u_g may not represent the true geostrophic wind component in the lower layer. Therefore, in case-2 this is improved.

6.2. Case-2

The estimation of the geostrophic wind components is improved in this case. Here the geostrophic wind components described in Section 5.2 are represented by the following equations:

$$u_g^* = \begin{cases} 0.24\ (1-z^*/3.9) & \text{for } z^* > 1.1 \\ 0.70\ (1-z^*/1.5) & \text{for } z^* \leq 1.1 \end{cases}, \tag{37}$$

$$v_g^* = 0.45\ (1-z^*/2.46). \tag{38}$$

The three calculated profiles of the down slope wind components are compared with the observed profile in Fig. 11a. The fit of these calculated wind components to the observed profile is improved. Moreover as in Fig. 11b the calculated cross slope wind components fit the observed components well except in the lower layer.

The calculated and observed wind hodographs, called wind spirals, are shown in Fig. 12. The solid line with black circles in Fig. 12 indicates observed values while the heavy solid line with open circles indicates calculated values with $\alpha=12$ and

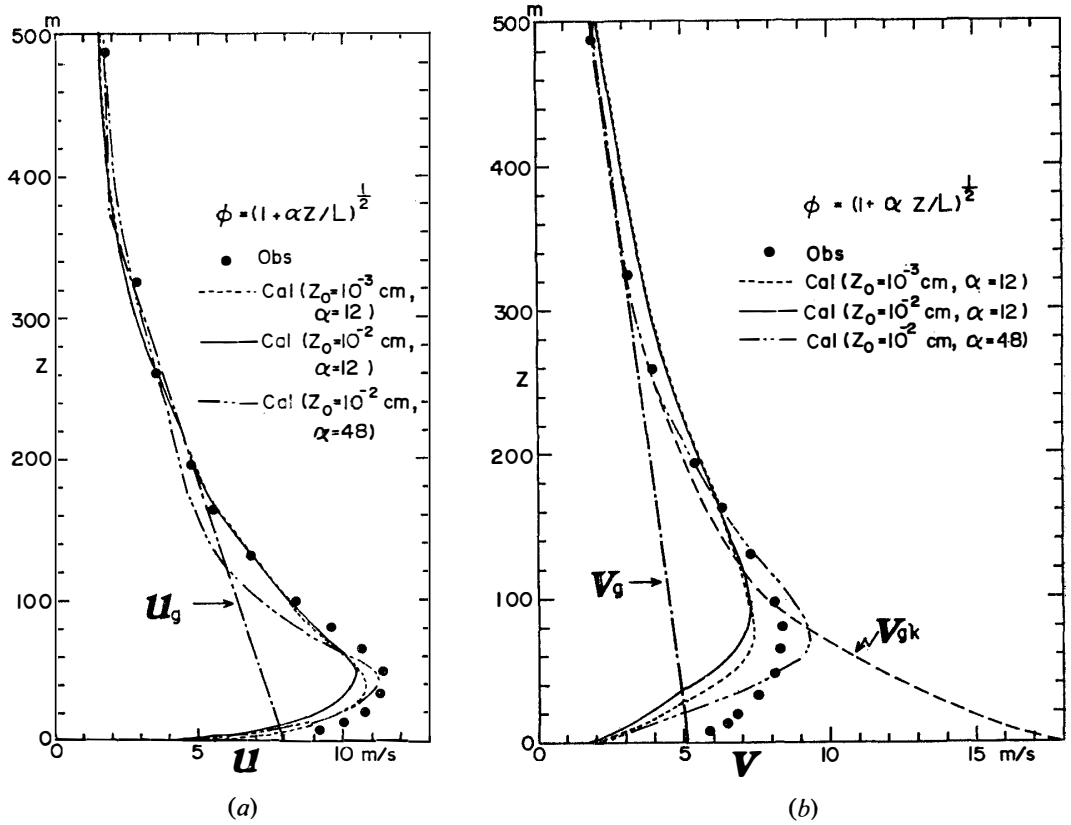

(*a*) (*b*)

Fig. 11. (*a*) *Calculated down slope wind component profiles vs. observed profile in case-2.* —·—: *Improved geostrophic wind component* (u_g).
(*b*) *Calculated cross slope wind component profiles vs. observed profile in case-2.* —·—: *Improved geostrophic wind component* (v_g), ----: v_{gk} ($=v_g+v_k$).

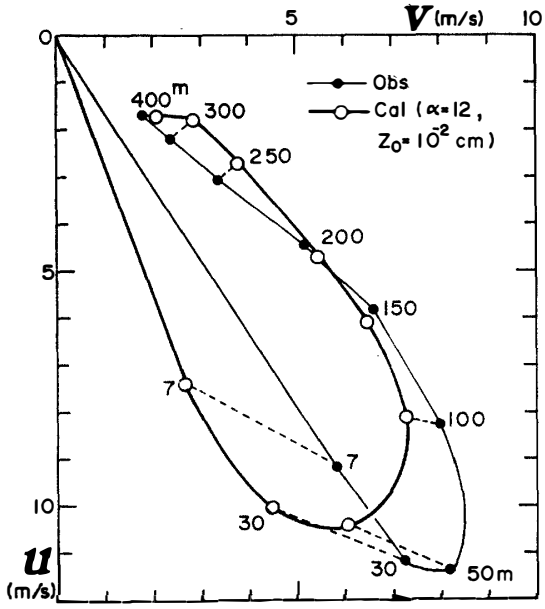

Fig. 12. Calculated wind spiral vs. observed spiral in case-2.

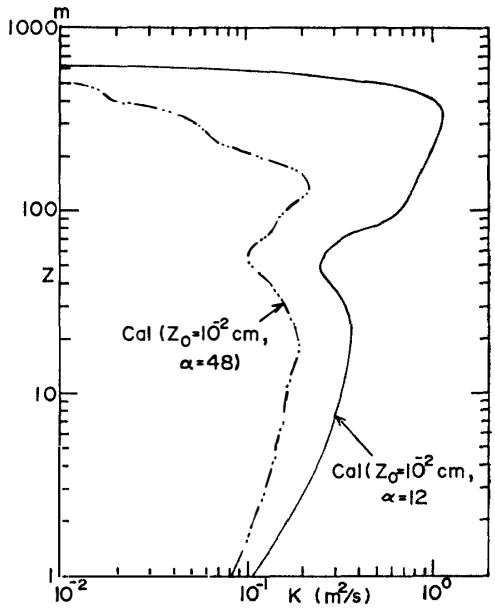

Fig. 13. Calculated eddy diffusivity (K) profiles in case-2.

$z_0 = 10^{-2}$ cm. The numbers indicate height above the snow surface. This calculated wind spiral fits the observed spiral well except below 100 m. It seems that the vertical profile of geostrophic wind component affects the numerical results considerably.

Predicted eddy diffusivity (K) profiles are shown in Fig. 13. The local minimum of K at 60–70 m is due to the maximum of wind velocity at that height.

The predicted profiles of friction velocity (u_*), stability (z/L) and non-dimensional wind shear function (ϕ) are shown in Fig. 14.

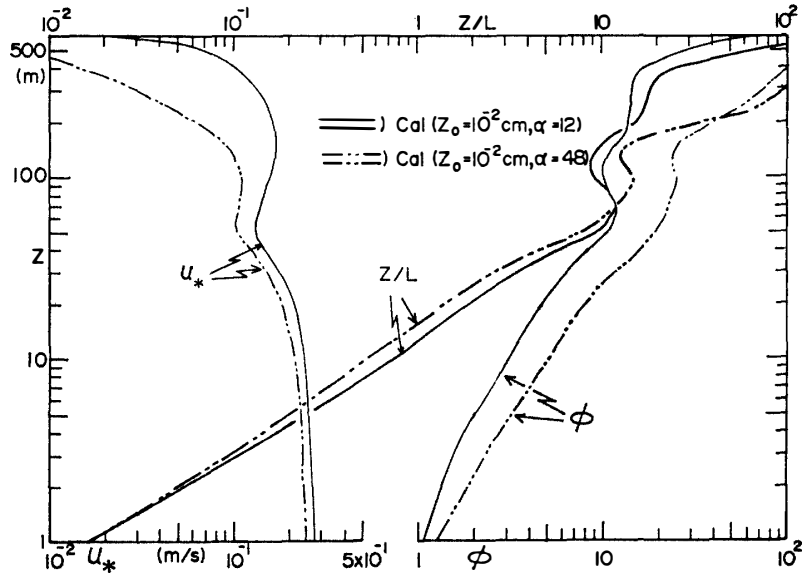

Fig. 14. Calculated profiles of friction velocity (u_*), stability (z/L) and non-dimensional wind shear function (ϕ) in case-2.

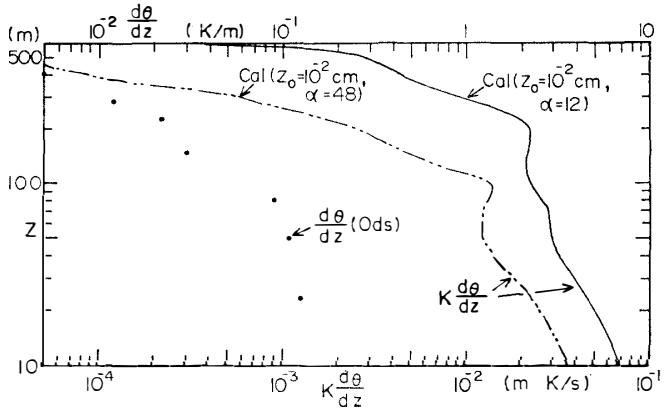

Fig. 15. Observed potential temperature gradient ($d\theta/dz$) profile and calculated heat flux ($K\ d\theta/dz$) profiles in case-2.

The observed potential temperature gradient ($d\theta/dz$) profile and predicted heat flux ($K d\theta/dz$) profiles are shown in Fig. 15.

The predicted results mentioned above are qualitatively reasonable.

7. Concluding Remarks

Aerological data observed at Mizuho Station during 1980 have been analyzed to select cases of typical katabatic wind profile. As a result 26 sets of data were obtained and averaged after normalization of vertical profiles of the potential temperature and two wind components.

Numerical simulation of the typical katabatic wind profile at Mizuho Station was done successfully by the one-dimensional model developed by ADACHI (1979) where not only the wind components but also the eddy diffusivity are unknown variables. Several comparisons of calculations with observations are shown.

Vertical profiles of eddy diffusivity, friction velocity and heat flux which were not observed at Mizuho Station during a typical katabatic wind are predicted by the present numerical simulation.

It is left to future study to estimate accurate vertical profiles of geostrophic wind component and the aerodynamical effect of the snow surface on the turbulence structure in the katabatic wind layer.

Acknowledgments

The authors are very grateful to Prof. J. KONDO and Associate Prof. N. YASUDA, Faculty of Science, Tohoku University, for valuable advice and suggestions.

The authors express their gratitude to Dr. S. OHTA, Dr. S. YOSHIDA, Dr. J. KOBAYASHI, Dr. S. MATSUMOTO, Mr. M. SHINYA and Mr. K. KUSANO, Japan Weather Association, for their continuing encouragement.

The authors are much indebted to Dr. O. CHIBA, Faculty of Science, Kochi University, for his constant advice and kindness.

It is a pleasure to acknowledge the hospitality and encouragement given by the staff of the National Institute of Polar Research.

The authors wish to thank Mrs. T. KOYAMA for the drawings.

References

ADACHI, T. (1979): Numerical simulation of katabatic wind profile at Syowa Station, Antarctica. Nankyoku Shiryô (Antarct. Rec.), **67**, 64–74.

ADACHI, T. (1982): Ekumansô ni tekiyô dekiru mujigen-ka fûsoku sheâ kansû (Non-dimensional wind shear function applicable to neutral or stable baroclinic atmosphere in the planetary boundary layer). Kyokuchi Kishô Yosoku Puroguramu no Shisutemu-ka no Kaihatsu Kenkyû Hôkokusho (Report of Research and Development of Forecasting Systems of Local Weather). Tokyo, Nihon Kishô Kyôkai (Japan Weather Assoc.), 44–60.

ADACHI, T. (1983): Numerical simulation of strong katabatic winds at Syowa and Mizuho Stations, Antarctica. Mem. Natl Inst. Polar Res., Spec. Issue, **29**, 50–60.

ADACHI, T. (1984a): Shamen-fû no kenkyû (Research of the slope wind). Kyokuchi Kishô Yosoku Puroguramu no Shisutemu-ka no Kaihatsu Kenkyû Hôkokusho (Report of Research and Development of Forecasting Systems of Local Weather). Tokyo, Nihon Kishô Kyôkai (Japan Weather Assoc.), 6–30.

ADACHI, T. (1984b): Analytical solutions of katabatic wind at Mizuho and Syowa Stations, Antarctica. Mem. Natl Inst. Polar Res., Spec. Issue, **34**, 54–61.

INOUE, J., NISHIMURA H. and SATOW, K. (1983): The climate of the interior of Mizuho Plateau. Mem. Natl Inst. Polar Res., Spec. Issue, **29**, 24–36.

KAWAGUCHI, S., KOBAYASHI, S., ISHIKAWA, N. and OHATA, T. (1982): Aerological soundings of the surface boundary layer at Mizuho Station, East Antarctica. Mem. Natl Inst. Polar Res., Spec. Issue, **24**, 77–86.

KOBAYASHI, S. (1978): Vertical structure of katabatic winds in Mizuho Plateau. Mem. Natl Inst. Polar Res., Spec. Issue, **7**, 72–80.

KOBAYASHI, S. and YOKOYAMA, K. (1976): Observations of the stationary katabatic winds in Mizuho Plateau, East Antarctica. Nankyoku Shiryô (Antarct. Rec.), **56**, 1–13.

KONDO, J., KANECHIKA, O. and YASUDA, N. (1978): Heat and momentum transfer under strong stability in the atmospheric surface layer. J. Atmos. Sci., **35**, 1012–1021.

OHATA, T., KOBAYASHI, S., ISHIKAWA, N. and KAWAGUCHI, S. (1981): Meteorological data at Mizuho Station, Antarctica in 1980. JARE Data Rep., **65** (Meteorol. 10), 93 p.

OHATA, T., ISHIKAWA, N., KOBAYASHI, S. and KAWAGUCHI, S. (1983): POLEX-South data, Part 4; Micrometeorological data at Mizuho Station, Antarctica in 1980. JARE Data Rep., **79** (Meteorol. 13), 374 p.

SASAKI, H. (1974): Higashi Nankyoku Mizuho Kansokukyoten ni okeru chijô kansoku (Surface meteorological observations at Mizuho Camp, East Antarctica). Nankyoku Shiryô (Antarct. Rec.), **50**, 21–28.

SASAKI, H. (1979): Preliminary study on the structure of the atmospheric surface layer in Mizuho Plateau, East Antarctica. Nankyoku Shiryô (Antarct. Rec.), **67**, 86–100.

SATOW, K., NISHIMURA, H. and INOUE, J. (1983): Glaciological data collected by the Japanese Antarctic Research Expedition in 1981. JARE Data Rep., **82** (Glaciol. 9), 81 p.

SHIMIZU, H., YOSHIMURA, A., NARUSE, R. and YOKOYAMA, K. (1978): Morphological feature of the ice sheet in Mizuho Plateau. Mem. Natl Inst. Polar Res., Spec. Issue, **7**, 14–25.

YAMADA, T. (1979): Prediction of the nocturnal surface inversion height. J. Appl. Meteorol., **18**, 526–531.

(*Received May 14, 1984*; *Revised manuscript received July 14, 1984*)